# The influence of slag compositional changes on the chemical degradation of magnesia-chromite refractories exposed to PbO-based non-ferrous slag saturated in spinel

L. Scheunis[1*], M. Campforts[2], P.T. Jones[1], B. Blanpain[1] and A. Malfliet[1]

[1]Department of Metallurgy and Materials Engineering, KU Leuven, Kasteelpark Arenberg 44, BE-3001 Leuven, Belgium

[2]Research & Development, Umicore, Watertorenstraat 33, BE-2250 Olen, Belgium

## Abstract

In non-ferrous metallurgy the refractory life is application dependent, typically going from several months up to 2 years or more. Slag engineering is widely used to reduce the dissolution rate of a refractory lining by forming a solid protection layer at the slag-lining interface, thereby increasing the lining's lifetime. The non-ferrous slag in this paper is engineered to form a protective spinel layer. This phase, however, only forms near and at the slag-lining interface, while deeper inside the sample forsterite grains are detected, resulting in direct contact between the still unsaturated slag and the magnesia-chromite refractory phases. At this position the MgO dissolution increases with a factor 3-4 compared with the slag-refractory interface, attacking the bonding between grains and decreasing the brick's mechanical strength. As this happens deeper inside the sample, the spalling risk increases. Strategies to simultaneously reduce refractory dissolution and spalling are discussed.

## Keywords

refractory wear; PbO slag; indirect dissolution; spinel formation; slag infiltration

## 1 Introduction

Ceramic magnesia-chromite refractory bricks are commonly used in non-ferrous smelting furnace linings because of their high melting point, good mechanical properties at elevated temperatures and their ability to withstand aggressive conditions [1-10]. Despite these properties, lining wear still occurs due to the combination of chemical, mechanical and thermal stresses, eventually requiring a replacement of the lining. Slag engineering is a common method used in industry to decrease the chemical degradation rate and thus to prolong the lining lifetime [4]. Two methods are typically used: (1) the bath composition can be saturated in the refractory components [11] or (2) the composition of the bath can be chosen to ensure the formation of a protective layer after reaction with the lining [12]. The first method reduces the thermodynamic driving force for dissolution, while the second creates a kinetic barrier for the dissolution as the refractory components have to diffuse through this newly formed solid layer.

* Corresponding author: *tel:* +32-16-321780; *fax:* +32-16-321991
*Email address:* lennart.scheunis@mtm.kuleuven.be (L. Scheunis).

In this paper the second approach is studied, focusing on how the formation of these protective phases, and thus the refractory dissolution, changes along the depth of a porous lining that has been infiltrated with liquid slag. Porous linings are widely used in pyrometallurgical reactors, especially batch processes as they are subjected to large changes in operating temperatures, to ensure that the lining is able to withstand the thermal and mechanical loads. This, however, comes at the cost of an accelerated chemical degradation, as the slag can infiltrate the porous brick, reacting with a larger part of the lining. The extent of the infiltration depends on the viscosity and wetting behavior of the slag system, and thus, for a given operating temperature, on its composition. PbO based, non-ferrous slag systems, for example, are known to easily and deeply infiltrate the refractory lining [13]. Other components are added to this slag to ensure the formation of new phases: alumina [9, 12] and iron oxide [14] because these components are known to form spinel phases [15-17] (of the type $(Mg,Fe^{2+})O.[Cr,Al,Fe^{3+}]_2O_3$), which in turn can lead to the indirect dissolution of the lining. Also $SiO_2$ is added as this component can lead to the formation of a second new phase (forsterite, $2MgO.SiO_2$ [18]), but not always forms a protective layer [13].

## 2 Experimental procedure

Constant temperature experiments were performed using standard static finger tests (see Figure 1) for different reaction times. The materials used consist of a commercially available fused grain rebonded magnesia-chromite brick and a synthetic $PbO$-$SiO_2$-$Al_2O_3$-$Fe_2O_3$-$CaO$ slag. Magnesia-chromite bricks are commonly used in both copper and lead smelters [2, 3]. A detailed description of the microstructure and the composition of all present phases for the used refractory sample can be found in Scheunis et al. [19]. The phase equilibria of a $PbO$-$SiO_2$-$Al_2O_3$-$Fe_2O_3$-$CaO$ slag have been extensively studied and the system has been optimized in FactSage [20]. Such a slag forms during the 2 stage production of lead from sulfur containing ores. First the ores are oxidized in contact with air to form the slag, which in a second stage is reduced to form Pb [16]. The used composition in this paper is chosen to ensure both a deep infiltration into the refractory as well as the formation of two different phases (forsterite and spinel) after reaction with the MgO from the slag. The slag is saturated in corundum ($(Al,Fe)_2O_3$) in order to limit the dissolution of the alumina crucible. The composition of the bath at the start of the experiment, determined using standardized XRF, is 47.5 wt% PbO, 11.9 wt% $SiO_2$, 21.2 wt% $Fe_2O_3$, 16.3 wt% $Al_2O_3$ and 0.8 wt% CaO. The properties of this slag are given in Table 1.

**Table 1: Properties of the used slag calculated using FactSage [21, 22] with a $pO_2$=0.21.**

| | |
|---|---|
| Liquidus temperature | 1425 °C |
| Solidus temperature | 725 °C |
| Primary phase | spinel |
| Phases present at 1300 °C | Liquid + corundum |
| Viscosity liquid fraction at 1300 °C | 0.409 Pa.s |

Prior to the experiment the refractory samples are cut in a bar shape (20x15x100 mm). The slag is produced by mixing different pure oxides powders in the desired ratio. The total weight of the mixture is 1.5 kg. It is heated in open air at a rate of 600 °C/hour in a 1 liter $Al_2O_3$ crucible using an induction furnace until a temperature of 1300 °C is reached. At the desired temperature, the

refractory finger, which is heated together with the crucible, is partially submerged into the liquid slag bath. After the required reaction time the sample is taken out of the bath and quenched in water in order to preserve the high temperature microstructure and composition in the best possible way. Three different reaction times are tested: 15 min, 1 hour and 3 hours.

After the test the finger is cut using a diamond saw. The section is made parallel and 1 cm below the slag bath line (see Figure 1). Before this section is analyzed it was embedded in an epoxy resin and polished. After coating the sample with a conducting carbon layer, both its microstructure and the composition of the different phases are analyzed using a fully quantitative EPMA-WDS (JEOL JXA-8530F) system operated using an acceleration voltage of 15 kV and a probe current of 15 nA. The oxygen content is not measured directly; instead the oxidation state of the element was selected a priori. Although both $Fe^{2+}$ and $Fe^{3+}$ can be present, only "$Fe_2O_3$" was selected for presentation purposes because the experiments are performed under a $pO_2$ of 0.21 making $Fe^{3+}$ the most likely form of iron.

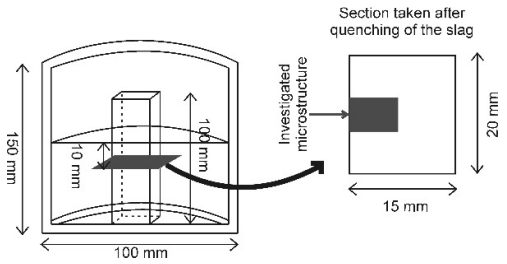


**Figure 1: Schematic representation of the experimental procedure showing the high temperature experimental setup, removal of the sample and the position of the investigated microstructure.**

# 3 Results

## 3.1 Microstructure

An overview image of the microstructure of the quenched sample after 15 min reaction time is shown in Figure 2. Besides the primary chromite (PC) and the fused grains (FG) present in the original microstructure, a new liquid phase (L) (appearing as the white phase) is observed, which penetrates the porous refractory sample under the influence of capillary forces. Despite the limited reaction time, the sample is already infiltrated right down to the center of the sample, indicating that the PbO based slag infiltrates very rapidly. As the sample after 15 min is already fully infiltrated, no additional infiltration will occur after 15 min and the difference between the different reaction times (15 min, 1h and 3h) lies in the changes in microstructure and slag composition, discussed in the rest of the paper.

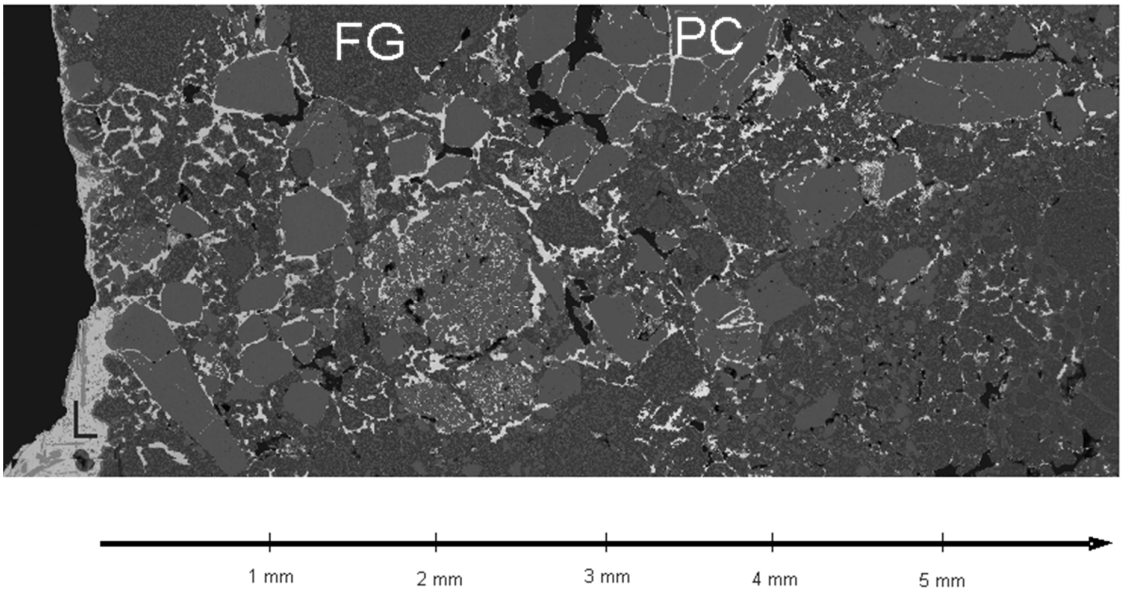


**Figure 2: BSE overview image of the microstructure after 15 min reaction time. With L: liquid; PC: primary chromite; FG: fused grain.**

Figure 3 shows a high magnification image of the interface between the refractory sample and the liquid slag bath, where a new spinel layer is observed on top of the original fused grain microstructure. To study the formation mechanism of this new spinel layer in more detail, compositional line scans are performed from the liquid bath along the newly formed spinel layer to the original fused grains for the 3 tested times. The results are shown in Figure 4. The positions for the line scan measurements are chosen on the largest grains, as far away from the open pores as possible, to limit the effect of liquid motion, caused by slag infiltration into the pores, on the growth of the new layers. In addition, only positions where the liquid-refractory interface runs parallel with the sample surface have been measured, making it possible to assume one dimensional growth of the new spinel phases.

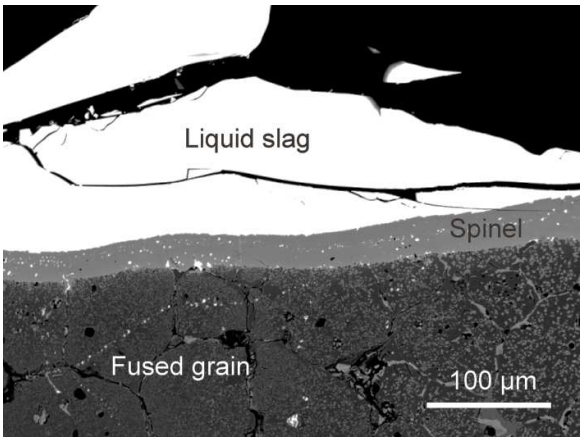


**Figure 3: Microstructure image of the interface between the sample and the liquid slag after 3 hours reaction time. A spinel layer is observed on the interface between the refractory material and the slag.**

For all measurements seen in Figure 4, three different phases can be distinguished: (1) the liquid slag, (2) the new spinel layer and (3) the original fused grain. The slag can be identified as it is the only phase containing PbO and $SiO_2$, while the periclase matrix of the fused grain consists of almost pure MgO. The transition between the different phases is shown by vertical lines in Figure 4, showing that the thickness of the new layer increases with time. This is also shown in Figure 6 where the thickness of the new spinel layer as a function of time is given, indicating an increase with √t. The growth rate (k), defined as $\Delta x^2/2t$, is thus 290.5 $\mu m^2/h$.

Figure 4 shows a decreasing $Al_2O_3$ concentration inside the new spinel layer from the liquid slag towards the fused grain in the refractory sample, while at the same time the MgO concentration increases. The "$Fe_2O_3$" concentration also decreases towards the original refractory, leveling off with time. Finally, $Cr_2O_3$ is detected in the interior of the new spinel phases, but only very locally.

Figure 5 shows the interaction between the slag and a chromite spinel grain, the second main phase in the original refractory sample. The same behavior for MgO and $Al_2O_3$ can be seen for the new spinel forming on top of the original primary chromite grain compared to the one forming on top of the original fused grain. The main difference is the presence of $Cr_2O_3$ throughout the entire new spinel phase, increasing from the slag towards the chromite spinel grain.

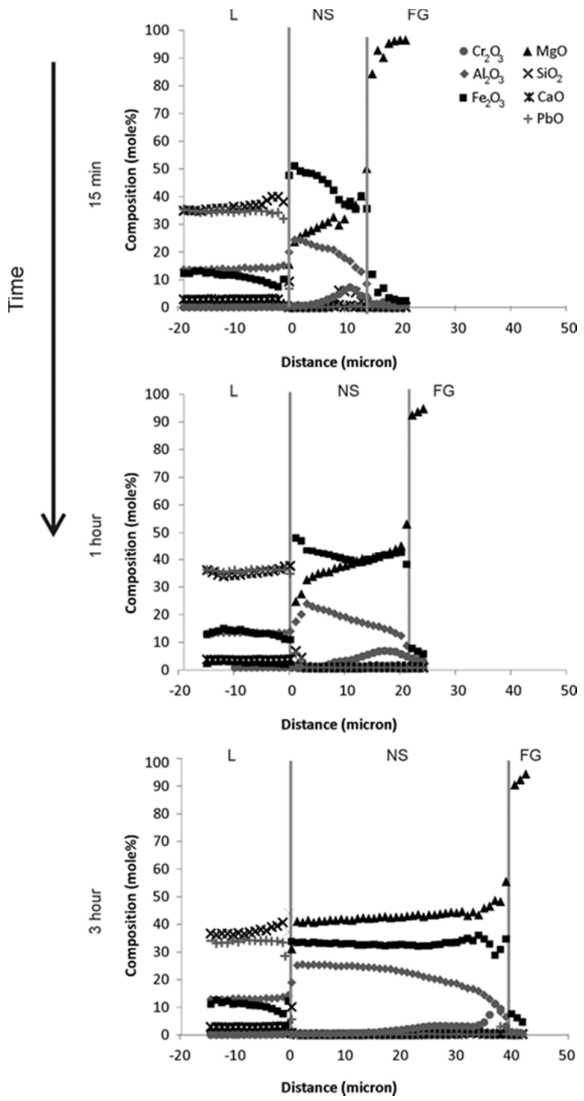


**Figure 4: Line scans showing the compositional variation as a function of distance over the spinel layer (NS) growing at the hot face between the liquid (L) and the fused grains (FG) for 3 different reaction times.**

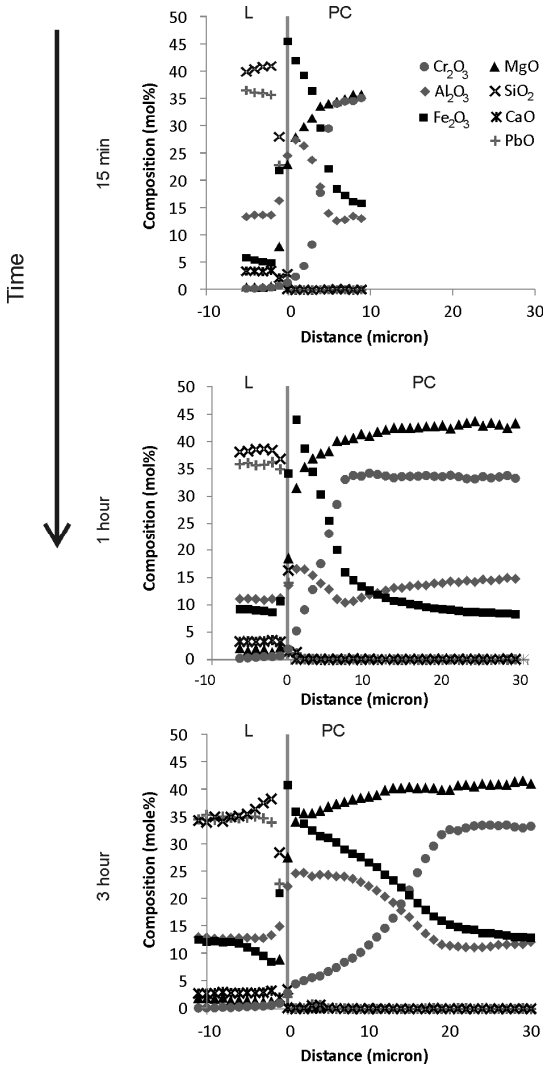


**Figure 5: Line scan showing the compositional variation as a function of distance between the liquid slag (L) and a primary chromite spinel grain (PC) after 3 different reaction times.**

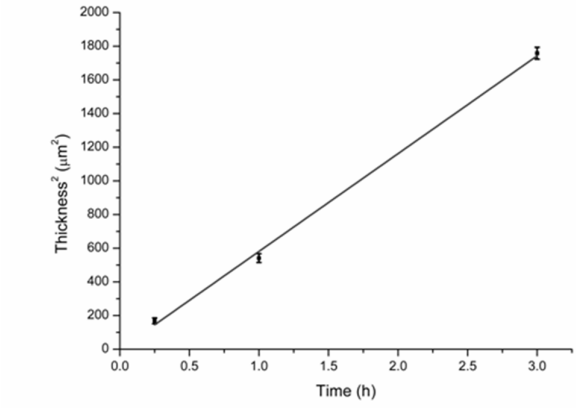


**Figure 6: Thickness variation of the new spinel layer as a function of the reaction time. The average thickness and the 95% confidence interval are shown for each reaction time (each based on at least 150 measurements). A linear fit of the average thickness values is shown with the following equation: $\Delta x^2=581t$ ($R^2 = 0.998$).**

Figure 7 shows detailed images of the microstructure at different depths from the refractory/slag interface for all three reaction times. Near the surface with the bath (0.5 mm), the new spinel (NS), also seen at the interface with the bath, forms a dense layer covering the entire original microstructure for all reaction times, while towards the center (3 mm), forsterite (F) is found as separate grains in all samples. At intermediate positions (1 and 2 mm) both the spinel and forsterite are present and the new spinel layer no longer covers the entire original microstructure. The forsterite grains grow with time, as seen at 3 mm from the bath/refractory interface.

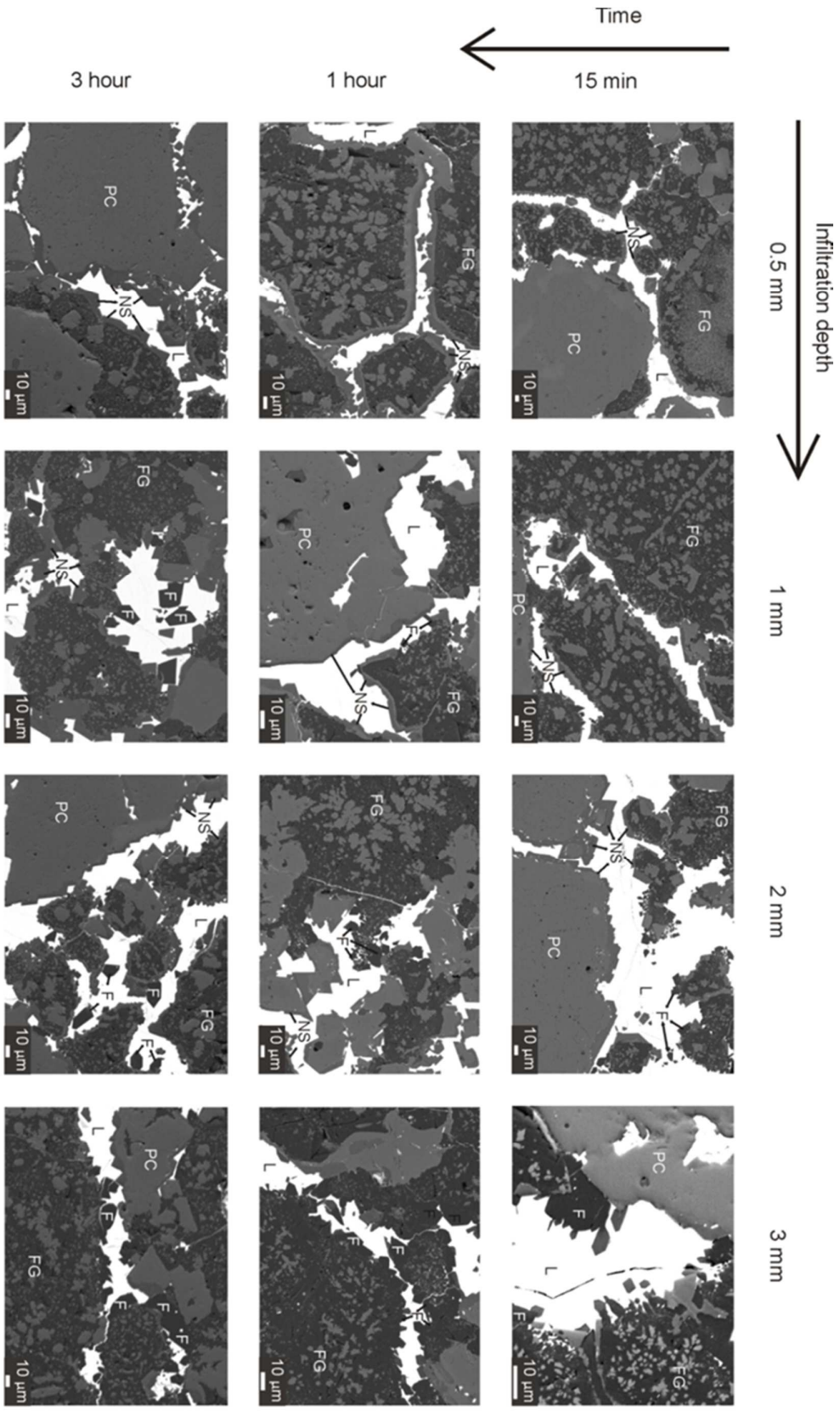


**Figure 7: Overview of the microstructure at different positions in the samples for the 3 tested times.**

## 3.2 Composition of the slag inside the sample

Figure 8 shows the variation of the composition of the liquid as a function of both distance and time. The results are all given in mole% to facilitate the analyses. Due to the increase in the PbO content of the slag and the high molecular weight of this component, the weight fraction of other (lighter) components automatically decreases. This can lead to wrong conclusions as it appears that components are (partially) removed from the slag, while in fact additional dissolution occurs. When the results are calculated to mole fractions, this problem is avoided. Figure 8 shows that the PbO content of the liquid increases while the $SiO_2$ content decreases with infiltration depth. This decrease, respectively increase, is, however, not uniformly distributed and can be divided into 3 main parts. In the first part (1), closest to the liquid bath, the concentration in PbO and $SiO_2$ remains relatively constant over time, although a slight decrease in $SiO_2$ and increase in PbO with distance can be seen. Deeper inside the sample, (2) the silica content decreases while the PbO concentration increases with depth. Finally, (3) in the center of the sample, the concentration for both remains constant again, albeit different from the concentration in zone 1. The composition in zones 1 and 3 does not change with time, only the position at which they occur varies over time.

Besides PbO and $SiO_2$, the two main components in the slag, Figure 8 also shows the variation in $Al_2O_3$ and MgO. The $Al_2O_3$ concentration shows a continuous drop with distance in zones 1 and 2, while the MgO concentration increases in zone 1 from near zero at the interface to a maximum value of 8-10 mole%, before decreasing again in zone 2. Both the $Al_2O_3$ and MgO concentrations reach a constant value in zone 3; 2-4 mole% for $Al_2O_3$ and 0-1 mole% for MgO.

Finally, "$Fe_2O_3$", $Cr_2O_3$ and CaO are also present inside the infiltrated slag. The iron content shows a drop at the hot face and remains constant at a value of about 6 mole% throughout the sample. The CaO content has a value between 4 and 6 mole% in zone 1 and 2, starting to drop at the end of zone 2 and reaching a constant value in zone 3 around 2 mole%. $Cr_2O_3$ is not detected in zones 1 and 2, but its concentration increases to about 2 mole% in zone 3.

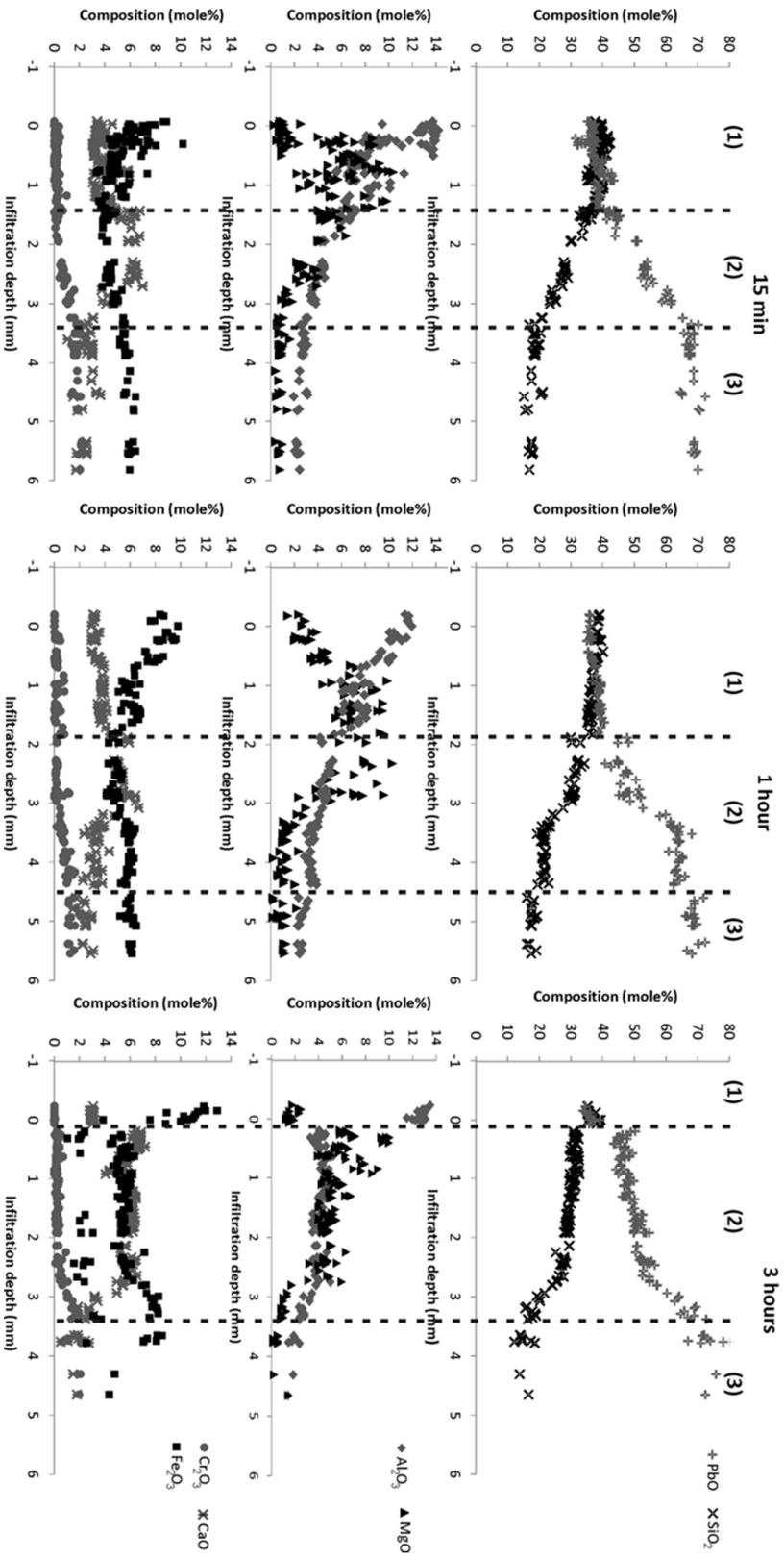


Figure 8: Composition of the liquid phase as a function of infiltration depth for different reaction times (measured using EMPA-WDS).

# 4 Discussion

According to Figure 3 and Figure 7 the new spinel forms in the first 2 mm of the samples. Figure 8 shows that at the same positions there is a drop in the $Al_2O_3$ and "$Fe_2O_3$" content of the infiltrating slag. The reaction forming these new spinel layers can thus be written as:

$$MgO_{refr} + Al_2O_{3\ slag} + "Fe_2O_3"_{slag} \rightarrow (Mg,Fe)\ [Al,Fe]_2O_4 \quad (1a)$$

$$MgO_{refr} + Cr_2O_{3\ refr} + Al_2O_{3\ slag,refr} + "Fe_2O_3"_{slag,refr} \rightarrow (Mg,Fe)\ [Al,Fe,Cr]_2O_4 \quad (1b)$$

This is further supported by the line scan results in Figures 4 and 5 where MgO, $Al_2O_3$, $Cr_2O_3$ and "$Fe_2O_3$" are the only components present in the new layer.

The spinel layer growing on top of the fused grain shows an MgO concentration gradient decreasing from the fused grain to the liquid bath, while $Al_2O_3$ shows the opposite trend. The growth rate of the spinel layer thus appears to be controlled by the counterdiffusion of MgO and $Al_2O_3$. The formation mechanism of a spinel layer forming on top of a pure MgO grain has been studied for the MgO-$Al_2O_3$ [23, 24], MgO-$Fe_2O_3$ [23] and MgO-$Cr_2O_3$ [25] systems, using only pure oxides. For all these systems the spinel layers grow by solid state diffusion of the cations through the newly formed solid spinel layer. Nightingale and Monaghan [26] showed that the same mechanism also holds when MgO reacts with liquid slag by studying the formation of a $MgAl_2O_4$ spinel between pure MgO and a synthetic CaO-$Al_2O_3$-$SiO_2$ slag, identifying the diffusion of $Mg^{2+}$ and $Al^{3+}$ through the spinel layer as the mechanism for additional growth. The spinel phase grows on both the MgO/spinel and spinel/$Al_2O_3$ (or slag) interface. The fused grains of the refractory, however, contain secondary chromite particles, with a different composition than the new spinel layer, which get absorbed into the growing layer. The most noteworthy difference is the presence of $Cr_2O_3$, which could explain why locally $Cr_2O_3$ is detected inside the new spinel layer.

Compared with the layers forming on the fused grains those forming on the original primary chromite systematically have $Cr_2O_3$ as an additional component. This component is known to diffuse much slower than $Al_2O_3$ [27] and therefore leads to a slow, continuous decrease in $Cr_2O_3$ from the chromite spinel towards the liquid bath, as seen in Figure 4. Because $Cr_2O_3$ takes the position of $Fe_2O_3$ and $Al_2O_3$ in the new spinel phase, the composition of the latter 2 components decreases towards the original chromite spinel.

The thickness variation for the new spinel layer as a function of time is fitted in Figure 6 according to a $\sqrt{t}$ dependency, typical for diffusion controlled growth of a phase, thereby confirming the diffusion controlled formation mechanism for the spinel layers suggested in the literature [23-26]. The obtained growth rate (k=290.5 $\mu m^2/h$) is, however, 50 times larger than the values in the open literature [26, 28, 29] for the growth rate of an $MgAl_2O_4$ spinel.

The new spinel phase (Mg,Fe)[Al,Fe]$_2O_4$ is not pure $MgAl_2O_4$ but can be seen as a combination of $MgAl_2O_4$ and magnetite ($Fe_3O_4$). Dieckmann and Schmalzried [30] studied the self-diffusion coefficient for Fe in magnetite ($Fe_3O_4$) and found a variation of several orders of magnitude as a function of $pO_2$, due to the creation of vacancies in the spinel lattice by the oxidation of $Fe^{2+}$ to $Fe^{3+}$. At room temperature magnetite is an inverse spinel [31, 32] but at higher temperatures $Fe^{2+}$ and $Fe^{3+}$ cations are randomly distributed between both the tetrahedral and octahedral sublattices. The vacancies most likely also have this distribution over both sublattices [33]. This leads to an increased

mobility for all the cations and can explain why the experimental growth rate of the $[Mg,Fe][Al,Fe]_2O_4$ spinel is so much higher compared to a pure $MgAl_2O_4$ spinel.

Due to the formation of new spinel layers, the concentration of spinel forming components ($Al_2O_3$, "$Fe_2O_3$") in the slag decreases with infiltration depth (see Figure 8), until the formation of new spinel is no longer possible. At this point forsterite becomes the dominant new phase. The formation of this phase requires the removal of silica from the bath, explaining the decrease in this component seen in Figure 8 in zone 2.

$$2MgO_{refr} + SiO_{2\ slag} \rightarrow Mg_2SiO_{4\ refr} \quad (5)$$

The dissolution rate of the refractory into the liquid bath is closely related to the phase formation. At the interface with the bath, the spinel acts as a protective layer slowing down the dissolution of MgO into the liquid slag. The diffusion profile in Figure 4 shows that MgO has to diffuse through the solid spinel layer before it can be dissolved in the liquid bath. The removal of "$Fe_2O_3$" and $Al_2O_3$ from the slag at the hot face means that insufficient driving force is available for new spinel formation to create a continuous protective layer inside the sample (see Figure 7, 1 mm). The MgO then makes direct contact with the slag, significantly increasing the dissolution of MgO, as seen in Figure 8, zone 1. Deeper inside the sample (zone 2 in Figure 8), the MgO content decreases again, despite direct contact between the slag and periclase. The reason for this is the removal of $SiO_2$ by forsterite formation, which, according to the PbO-$SiO_2$-MgO phase diagram, [18], lowers the MgO solubility. At the end of zone 2, the CaO concentration in the slag also decreases, because the formed forsterite also contains some CaO.

When $Al_2O_3$, "$Fe_2O_3$", $SiO_2$ and CaO react with the refractory to form new phases, the slag gets enriched in PbO. The $Cr_2O_3$ concentration in the slag also increases towards the center of the sample, indicating that the chromite phase is attacked, as $Cr_2O_3$ is only present in this phase. The $Cr_2O_3$ increase only occurs in zone 3, together with a $SiO_2$ drop, which would suggest that the removal of $SiO_2$ increases the $Cr_2O_3$ solubility for high PbO slag systems. In order to validate this hypothesis, thermodynamic calculations are performed using the FactSage FTOxid database [22] to predict the effect of $SiO_2$ removal on the $Cr_2O_3$ solubility of a $Cr_2O_3$ saturated slag. The results are shown in Figure 9 together with the experimental data shown in Figure 8 rescaled to only PbO-$SiO_2$-$Cr_2O_3$. Figure 9 shows that for both the calculations and the measured data the $Cr_2O_3$ solubility increases with a decreasing $SiO_2$ content. The effect of other components (in this case $Al_2O_3$) in the slag decreases the $Cr_2O_3$ solubility, but does not change the increasing trend for the $Cr_2O_3$ solubility with decreasing $SiO_2$ content in the slag.

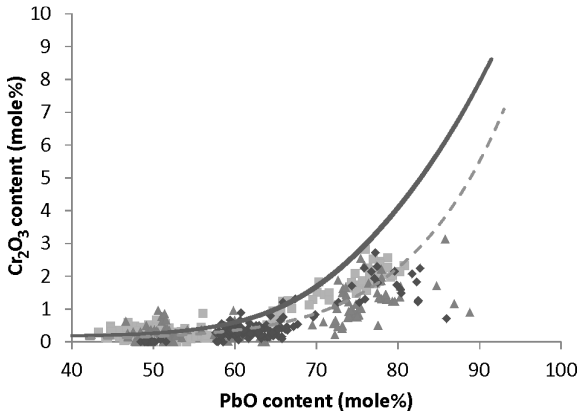


**Figure 9: $Cr_2O_3$ solubility in a PbO-$SiO_2$-$Cr_2O_3$ slag at 1300 °C and $pO_2$=0.21 calculated using FactSage (full line) and with 10 mole% $Al_2O_3$ added to the liquid slag (dotted line). The experimental data given in Figure 8 are also shown, rescaled to only PbO, $SiO_2$ and $Cr_2O_3$ to compare with the calculations. (with ■: 15 min ▲: 1h and ♦:3h reaction time).**

# 5 Effect on the overall degradation of a refractory lining

The experimental results indicate that the formation of a protective spinel layer near the hot face lowers the dissolution of MgO from the refractory into the liquid slag bath. Figure 10 gives a conceptual description of how the formation of such a protective layer can affect the overall degradation in a refractory lining. The original refractory sample (Figure 10a) consists of different grains which are sintered together with open pores between them. The bonds between the different grains give the refractory bricks their mechanical strength. When such a brick comes into contact with liquid slag (Figure 10b), the refractory components start to dissolve into the slag. This dissolution is typically the fastest at the hot face as the lining is in contact with a large amount of slag, constantly being replaced by fresh, unsaturated liquid by the movement of the bath. Deeper inside the sample the infiltrated liquid is saturated by the previous reactions and no further dissolution occurs. By forming a protective layer at the hot face (Figure 10c), the MgO dissolution at the hot face decreases and is shifted to the interior of the lining where the movement of the bath is less pronounced and, furthermore, the amount of liquid slag in contact with the refractory phases is significantly lower, reducing the chemical attack. The main disadvantage of MgO dissolution inside the sample is that the attack of the bonding between the grains now occurs much deeper in the sample, resulting in a locally weakened structure of the lining. When this part is no longer able to withstand the applied mechanical or thermal loads, an entire part of the lining, including the protective spinel layer, may spall off and the cycle can start again on the newly exposed part of the lining.

For $SiO_2$ containing systems, forsterite bursting [34] is a common cause of spalling. It is caused by internal stresses after formation of forsterite phases. When forsterite forms near the hot face (Figure 10d), the part of the lining affected by spalling is limited. Deeper in the sample, the liquid is typically depleted in $SiO_2$ and no more forsterite is formed there. When a protective spinel layer forms near the hot face (Figure 10e), the $SiO_2$ cannot react with the refractory grains near the hot face and is transported deeper into the refractory with the infiltrating liquid slag. Forsterite therefore forms much deeper inside the lining, when the protective layer no longer forms. In this case, the internal stresses caused by the forsterite can lead to the spalling of a much larger part of the lining.

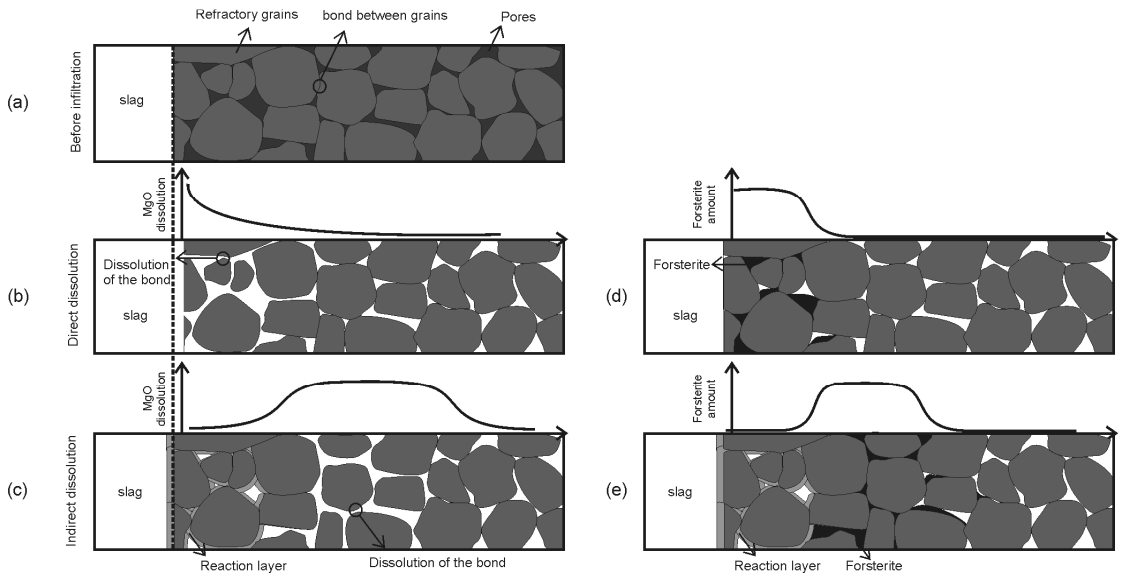


**Figure 10: Conceptual description of the effect of a protective reaction layer on the dissolution of the refractory grains (b-c) and on the formation of a second phase (forsterite in this case, d-e).**

A possible way to minimize the overall degradation is further slag engineering to limit the MgO dissolution. The easiest way to do this is to saturate the slag in MgO. However, the MgO solubility will depend on the slag composition, which in turn (as seen from the experimental results) changes throughout the brick. If too much MgO is added to the slag bath, it will start reacting with the $Al_2O_3$ and "$Fe_2O_3$" components, forming spinel phases in the slag, which could be undesirable as they increase slag viscosity.

Alternatively, external cooling can be applied to the lining. The resulting temperature gradient lowers the growth rate of the spinel layer inside the sample, slowing down the removal of spinel forming components from the infiltrating liquid. This would mean that a (thinner) protective layer forms in a larger part of the lining. Direct contact between the refractory phases and the infiltrating liquid, therefore, occurs deeper inside the sample at a lower temperature and, thus, at a lower solubility of the refractory components into the liquid slag, reducing the spalling risk. This effect can be further enhanced by combining it with slag engineering: by modifying the slag to limit iron (or other multivalent) cations inside the spinel layer, the vacancy concentration (and thus the growth rate) will decrease, allowing even more spinel forming components to be transported into the interior of the lining.

## 6 Conclusions

In this paper the interaction between a magnesia-chromite refractory sample and a synthetic PbO-$SiO_2$-$Fe_2O_3$-$Al_2O_3$-CaO non-ferrous slag is studied using constant temperature finger experiments at 1300 °C for 3 different reaction times. The main conclusions are:

- During the infiltration of the liquid slag into the porous refractory sample, the reaction between the slag and the refractory leads to the formation of new interfacial layers, corroborating the importance of local equilibria with respect to refractory wear [35]. In the studied samples two different types were formed: a forsterite and a spinel layer. The spinel forms closest to the hot face while the forsterite is present deeper inside the brick.

- The slag compositional evolution is closely related to the phase formation and therefore also changes with position. Near the hot face the spinel formation requires $Al_2O_3$ and "$Fe_2O_3$" thereby removing them from the slag. When insufficient $Al_2O_3$ and "$Fe_2O_3$" remain in the infiltrating slag to form new spinel layers, forsterite is formed decreasing the $SiO_2$ content of the slag. The removal of $Al_2O_3$, "$Fe_2O_3$" and $SiO_2$ from the slag results in a PbO enriched slag in the center of the sample.

- A spinel layer forms at the interface between the slag and the refractory sample, leading to indirect dissolution of the refractory lining as the MgO has to diffuse through the solid spinel layer to dissolve into the slag, slowing down the wear of the lining.

- The dissolution of MgO from the refractory phases is significantly higher inside the lining than at the interface with the bath because the continuous protective spinel layer no longer forms. The MgO concentration in the slag decreases again further inside the lining as the MgO solubility decreases with the $SiO_2$ concentration.

- The $Cr_2O_3$ dissolution from the chromite spinel phases only occurs deep inside the sample when the slag contains primarily PbO.

- The formation of a protective spinel layer on top of the refractory phases slows down the dissolution of MgO into the liquid bath but at the same time increases the risk of spalling by weakening the structure of the refractory deeper inside the lining, which can lead to failure during thermo-mechanical loads. There are two main reasons for the loss of mechanical strength: (1) dissolving of the bond between the different refractory grains and/or (2) internal stresses caused by the formation of new phases inside the lining. Engineering the slag to minimize the refractory wear rate, therefore, not only has to consider the dissolution rate at the hot face, which can be reduced by the formation of a protective layer, but also needs to consider the effect this has on the spalling behavior of the lining.

## 7 Acknowledgement

This research was supported by the Agency for Innovation by Science and Technology in Flanders and by Umicore (IWT Baekeland mandate 100700). The authors also like to thank Saskia Bodvin, Mieke Van Dingenen and Jef Vets from Umicore for their help with the planning and execution of the experimental part. We also gratefully acknowledge support for the FEG-EPMA measurements from the Hercules Foundation (project ZW09-09).

## 8 References

1. Barthel H., *Wear of chrome magnesite bricks in copper smelting furnaces.* Inter-Ceram, 1981. **30**: p. 250-5.

2. Köffel M. and Taschler T., *Refractories for the copper and lead industry.* World of Metallurgy - ERZMETALL, 2006. **59**(3): p. 133-42.
3. Taschler T. *Refractory Materials for the Copper and Lead industry*. in *Tehran International Conference on Refractories*. 2004. Tehran, Iran.
4. Malfliet A., Lotfian S., Scheunis L., Petkov V., Pandelaers L., Jones P. T. and Blanpain B., *Degradation mechanisms and use of refractory linings in copper production processes: A critical review.* Journal of the European Ceramic Society. **34**(3): p. 849-76.
5. Petkov V., Jones P. T., Boydens E., Blanpain B. and Wollants P., *Chemical corrosion mechanisms of magnesia-chromite and chrome-free refractory bricks by copper metal and anode slag.* Journal of the European Ceramic Society, 2007. **27**(6): p. 2433-44.
6. Jones P. T., Blanpain B., Wollants P., Ding R. and Hallemans B., *Degradation mechanisms of magnesia-chromite refractories in vacuum-oxygen decarburisation ladles during production of stainless steel.* Ironmaking & Steelmaking, 2000. **27**(3): p. 228-37.
7. Jones P. T., Desmet D., Guo M. X., Durinck D., Verhaeghe F., Van Dyck J., Liu J. H., Blanpain B. and Wollants P., *Using confocal scanning laser microscopy for the in situ study of high-temperature behaviour of complex ceramic materials.* Journal of the European Ceramic Society, 2007. **27**(12): p. 3497-507.
8. Jones P. T., Vleugels J., Volders I., Blanpain B., Van der Biest O. and Wollants P., *A study of slag-infiltrated magnesia-chromite refractories using hybrid microwave heating.* Journal of the European Ceramic Society, 2002. **22**(6): p. 903-16.
9. Guo M., Jones P. T., Parada S., Boydens E., Van Dyck J., Blanpain B. and Wollants P., *Degradation mechanisms of magnesia-chromite refractories by high-alumina stainless steel slags under vacuum conditions.* Journal of the European Ceramic Society, 2006. **26**(16): p. 3831-43.
10. Lee W. E. and Zhang S., *Melt corrosion of oxide and oxide-carbon refractories.* International Materials Reviews, 1999. **44**(3): p. 77-104.
11. Van Ende M.-A., Guo M., Jones P. T., Blanpain B. and Wollants P., *Degradation of MgO-C refractories by MnO-rich stainless steel slags.* Ceramics International, 2009. **35**(6): p. 2203-12.
12. Liu J., Guo M., Jones P. T., Verhaeghe F., Blanpain B. and Wollants P., *In situ observation of the direct and indirect dissolution of MgO particles in CaO-Al2O3-SiO2-based slags.* Journal of the European Ceramic Society, 2007. **27**(4): p. 1961-72.
13. Scheunis L., Fallah Mehrjardi A., Campforts M., Jones P. T., Blanpain B. and Jak E., *The effect of phase formation during use on the chemical corrosion of magnesiaâ€“chromite refractories in contact with a non-ferrous PbOâ€“SiO2 based slag.* Journal of the European Ceramic Society. **34**(6): p. 1599-610.
14. Yan S., Sun S. and Jahanshahi S., *Reactions of dense MgO with calcium ferrite-based slags at 1573 K.* Metallurgical and Materials Transactions B-Process Metallurgy and Materials Processing Science, 2005. **36**(5): p. 651-6.
15. Jak E. and Hayes P. C., *The effect of the CaO/SiO2 ratio on the phase equilibria in the ZnO-"Fe2O3"-(PbO+CaO+SiO2) system in air: CaO/SiO2=0.1, PbO/(CaO+SiO2)=6.2, and CaO/SiO2=0.6, PbO/(CaO+SiO2)=4.3.* Metallurgical and Materials Transactions B-Process Metallurgy and Materials Processing Science, 2003. **34**(4): p. 369-82.
16. Jak E. and Hayes P. C., *Experimental study of phase equilibria in the PbO-ZnO-"Fe2O3"-CaO-SiO2 system in air for high lead smelting slags (CaO/SiO2=0.35 and PbO/(CaO+SiO2)=5.0 by weight).* Metallurgical and Materials Transactions B-Process Metallurgy and Materials Processing Science, 2002. **33**(6): p. 817-25.
17. Jak E. and Hayes P. C., *Experimental liquidus in the PbO-ZnO-"Fe2O3"-(CaO+SiO2) system in air, with CaO/SiO2=0.35 and PbO/(CaO+SiO2)=3.2.* Metallurgical and Materials Transactions B-Process Metallurgy and Materials Processing Science, 2002. **33**(6): p. 851-63.
18. Chen S., Zhao B., Jak E. and Hayes P. C., *Experimental study of phase equilibria in the PbO-MgO-SiO2 system.* Metallurgical and Materials Transactions B-Process Metallurgy and Materials Processing Science, 2001. **32**(1): p. 11-6.

19. Scheunis L., Fallah Mehrjardi A., Campforts M., Jones P. T., Blanpain B. and Jak E., *The effect of phase formation during use on the chemical corrosion of magnesia–chromite refractories in contact with a non-ferrous PbO–SiO2 based slag.* Journal of the European Ceramic Society, 2014. **34**(6): p. 1599-610.
20. Jak E., Degterov S., Zhao B., Pelton A. and Hayes P. *Coupled experimental and thermodynamic modelling study of the system PbO-ZnO-FeO-Fe2O3-CaO-SiO2-Al2O3 for lead and zinc smelting*. in *Zinc and Lead Processing*. 1998. Canadian Institute of Mining, Metallurgy and Petroleum.
21. Bale C., Chartrand P., Degterov S. A., Eriksson G., Hack K., Ben Mahfoud R., Melancon J., Pelton A. D. and Petersen S., *FactSage thermochemical software and databases.* Calphad-Computer Coupling of Phase Diagrams and Thermochemistry, 2002. **26**(2): p. 189-228.
22. Bale C. W., Belisle E., Chartrand P., Decterov S. A., Eriksson G., Hack K., Jung I. H., Kang Y. B., Melancon J., Pelton A. D., Robelin C., and Petersen S., *FactSage thermochemical software and databases - recent developments.* Calphad-Computer Coupling of Phase Diagrams and Thermochemistry, 2009. **33**(2): p. 295-311.
23. Carter R. E., *MECHANISM OF SOLID-STATE REACTION BETWEEN MAGNESIUM OXIDE AND ALUMINUM OXIDE AND BETWEEN MAGNESIUM OXIDE AND FERRIC OXIDE.* Journal of the American Ceramic Society, 1961. **44**(3): p. 116-20.
24. Sako E. Y., Braulio M. A. L., Zinngrebe E., van der Laan S. R. and Pandolfelli V. C., *Fundamentals and applications on in situ spinel formation mechanisms in Al2O3-MgO refractory castables.* Ceramics International. **38**(3): p. 2243-51.
25. Nagata K., Nishiwaki R., Nakamura Y. and Maruyama T., *KINETIC MECHANISMS OF THE FORMATIONS OF MGCR2O4 AND FECR2O4 SPINELS FROM THEIR METAL-OXIDES.* Solid State Ionics, 1991. **49**: p. 161-6.
26. Nightingale S. A. and Monaghan B. J., *Kinetics of Spinel Formation and Growth during Dissolution of MgO in CaO-Al2O3-SiO2 Slag.* Metallurgical and Materials Transactions B-Process Metallurgy and Materials Processing Science, 2008. **39**(5): p. 643-8.
27. Suzuki A. M., Yasuda A. and Ozawa K., *Cr and Al diffusion in chromite spinel: experimental determination and its implication for diffusion creep.* Physics and Chemistry of Minerals, 2008. **35**(8): p. 433-45.
28. Zhang P., Debroy T. and Seetharaman S., *Interdiffusion in the MgO-Al2O3 spinel with or without some dopants.* Metallurgical and Materials Transactions a-Physical Metallurgy and Materials Science, 1996. **27**(8): p. 2105-14.
29. Whitney W. P. and Stubican V. S., *INTERDIFFUSION STUDIES IN SYSTEM MGO-AL2O3.* Journal of Physics and Chemistry of Solids, 1971. **32**(2): p. 305-&.
30. Dieckmann R. and Schmalzried H., *DEFECTS AND CATION DIFFUSION IN MAGNETITE .1.* Berichte Der Bunsen-Gesellschaft-Physical Chemistry Chemical Physics, 1977. **81**(3): p. 344-7.
31. C.G. Shull E. O. W., W.C. Koehler, *Neutron scattering and polarization by ferromagnetic materials.* Physical review, 1951. **84**(5): p. 912-21.
32. Verwey EJ H. P., Romeijn FC, *Physical properties and cation arrangement of oxides with spinel structures II Electronic conductivity.* The journal of chemical physics, 1947. **15**(4): p. 181-7.
33. Dieckmann R. and Schmalzried H., *DEFECTS AND CATION DIFFUSION IN MAGNETITE(II).* Berichte Der Bunsen-Gesellschaft-Physical Chemistry Chemical Physics, 1977. **81**(4): p. 414-9.
34. Gregurek D., Majcenovic C., Sparing A. and Kirschen M., *Forsterite bursting in magnesia chromite bricks - two case studies from lead and copper smelting furnaces.* RHI Bulletin, 2011(2): p. 49-53.
35. Lee W. E., Argent B. B. and Zhang S. W., *Complex phase equilibria in refractories design and use.* Journal of the American Ceramic Society, 2002. **85**(12): p. 2911-8.